

Modeling the Clutter Reflection Suppression Algorithm in Synthetic-Aperture Radar

Leonid G. Dorosinskiy¹ and Andrew A. Kurganski¹

Ural Federal University, pr. Mira, 19, Yekaterinburg, 620002, Russian Federation
k-and92@mail.ru

Abstract. Modeling the clutter reflection suppression algorithm in synthetic-aperture radar is considered in the article. The proposed algorithm allows one to increase the signal detection efficiency with closely located sources of clutter due to the use of *a priori* data of static objects of the infrastructure.

Keywords: Optimal detection algorithm, SAR, clutter suppression

1 Introduction

The forming problem of the optimal algorithm for signal detection in the radar with synthesized aperture (SAR) under the presence of the clutter reflections from the local objects and the design of the efficiency estimation method of such detection are the main problems in the development air and satellite observational platforms for remote earth and water surfaces sensing system.

2 Algorithm development

Devoted to the problems of signal processing within the SAR papers [1–3] pay great attention to research of the detection algorithms under clutter impact caused by the reflection from the underlying surface and noises. A SAR antenna pattern in some practical situations (along with the valid signal reflected from the multiple-unit target) has powerful clutter signals produced by the reflections from the clutter objects. Therefore, in these cases the processing algorithm should be formed accounting both the distribution target character and the clutter presence. Determination of the main principles of algorithm construction and the analysis methods present the content of this paper. Suppose the side-looking radar moves along the linear path. The range resolution cell has the target and clutter signals formed by the separate reflectors, which are distant at $d_i^t (i = \overline{1, n})$ and $d_i^c (i = \overline{1, N})$ from the coordinate origin with the Δt step, and n and N are the numbers of the target and clutter reflectors respectively (Fig. 1). Under the discrete time processing, the vector of the observed data is presented in the following form:

$$Y = \beta_T A_T + \beta_C A_C + N_N \quad (1)$$

$$\beta_T = \begin{pmatrix} X(d_{1,1}^t), X(d_{2,1}^t), \dots, X(d_{n,1}^t) \\ X(d_{1,2}^t), X(d_{2,2}^t), \dots, X(d_{n,2}^t) \\ \vdots \\ X(d_{1,M}^t), X(d_{2,M}^t), \dots, X(d_{n,M}^t) \end{pmatrix} \quad (2)$$

where

$$X(d_{n,k}^t) = \left\| \exp(-j \frac{4\pi}{\lambda R_0} d_n r_k) \right\| \quad (3)$$

is the phase signal distribution reflected from i -target element on the points of synthesized aperture with the coordinates r_k , $k = 1, \bar{M}$ (λ is the wavelength); A_T and A_C are $(n \times 1)$ and $(N \times 1)$ vectors of complex target and clutter amplitudes which are normal random variables with zero mean and dispersions $\sigma_{T_i}^2$ and $\sigma_{C_i}^2$ respectively; matrix β_C is determined similarly to (2) and (3), N_N is the complex amplitude vector of gaussian noise.

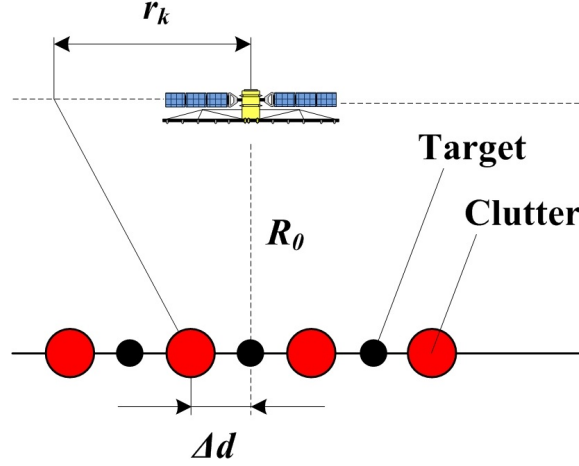


Fig. 1. Task geometry

Recording the observed data in the form (1), the quadric form of sufficient statistics for the detection of the target signal is

$$\alpha = Y^{*T} \Theta Y, \quad (4)$$

where $\Theta = R_C^{-1} - R_{TC}^{-1}$ is the processing weight function,

$$R_{TC} = \beta_T Q_T \beta_T^{*T} + R_C^{-1}, \quad (5)$$

$$R_C = \beta_C Q_C \beta_C^{*T} + R_N, \quad (6)$$

are the correlation matrices of vector (1) with and without the target signal respectively

$$Q_T = \text{diag}(\sigma_{T_1}^2, \dots, \sigma_{T_n}^2), \quad (7)$$

$$Q_C = \text{diag}(\sigma_{C_1}^2, \dots, \sigma_{C_N}^2), \quad (8)$$

$$R_N = \sigma_N^2 E \quad (9)$$

where $*$ is a complex conjugation, T is a transpose sign, E is the identity matrix with the noise dispersion $\sigma_N^2 = 1$. Using Woodbury formula for the determination of the optimal weight function the equation of the sufficient statistics derives as

$$\alpha = Z P Z^{*T}, \quad (10)$$

where

$$P = (E + Q_T \beta_T^{*T} R_C^{-1} \beta_T)^{-1} Q_T, \quad (11)$$

$$R_C^{-1} = R_N^{-1} - R_N^{-1} \beta_C (E + Q_C \beta_C^{*T} R_N^{-1} \beta_C)^{-1} Q_C \beta_C^{*T} R_N^{-1}, \quad (12)$$

$$Z = Y^T R_C^{-1} \beta_T^* = Y^T X^*(d_i^t) - \sum_{l=1}^N \chi_{li} Y^T X^*(d_l^c), \quad (13)$$

$$\chi_{li} = \sum_{t=1}^n \rho_{lt} X^T(d_l^c) X^*(d_i^t) \quad (14)$$

where ρ_{lt} is the matrix (11) element.

The schematic structure with the optimal algorithm (10) is shown on Fig. 2. The main functional operation in (13) is

$$Y^T X^*(d_i) = \sum_{k=1}^M \exp(-j \frac{4\pi}{\lambda R_0} d_i^t r_k) \quad (15)$$

that presents the chirp demodulation and the discrete Fourier transform (DFT) estimated for the spatial frequencies $2d_i/\lambda R_0$ that corresponding to all elements of target (clutters).

3 Algorithm analysis

The relative gain of the optimal processing in comparison with the traditional one in SAR does not allow one to estimate the absolute values of the detection characteristics with multiple-unit sources of signals and clutters. On the other hand, the exact calculation of these characteristics is connected with the significant calculation difficulties caused in the determination and integration of distributed statistics (10). Therefore, the efficiency estimation of the considered algorithm uses the method based on the Chernoff bound [3], according to which the detection and false alarm probabilities are counted the formulas

$$P_D = -\exp[\gamma(\nu(s) + (1-s)(\dot{\nu}(s) + 0.5(1-s)^2)\ddot{\nu}(s))] \times \text{erfc}[(1-s)\sqrt{\gamma\ddot{\nu}(s)}], \quad (16)$$

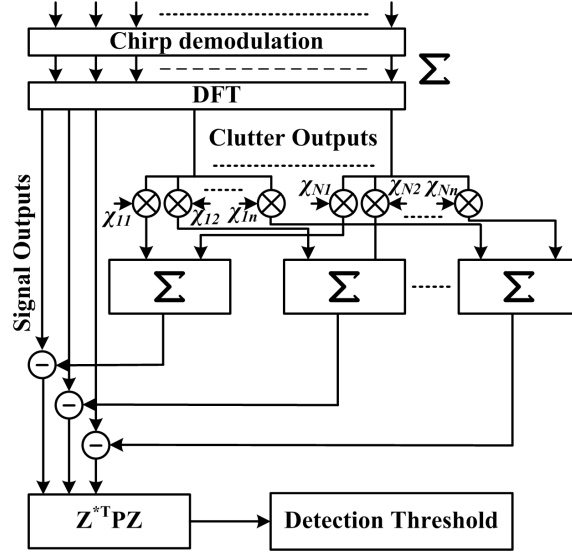


Fig. 2. Optimal algorithm flowchart

$$P_F = \exp[\gamma(\nu(s) + s\dot{\nu}(s) + 0.5s^2\ddot{\nu}(s))] \times \text{erfc}[s\sqrt{\gamma\ddot{\nu}(s)}], \quad (17)$$

where

$$\nu(s) = \ln \int_{-\infty}^{\infty} \dots \int_{-\infty}^{\infty} P \left[\left(\frac{Y}{T+C} \right) \right]^2 [P(Y/C)]^{1-s} dY, \quad (18)$$

and $\dot{\nu}(s)$ and $\ddot{\nu}(s)$ are the first and second derivatives of (18), $s = 0 \dots 1$ is the dummy argument, γ is the number of independent tests (for SAR γ is the nlook, *e.g.* the number of used frequencies with multi frequency probing or the number of non-coherent summed synthesized images for partly coherent SAR working mode), $P(Y/(T+C)), P(Y/C)$ are the probability densities of the observed vector under presence or absence of the target signal.

According to the case presented in the paper, formula (18) has the following form:

$$\nu(s) = -0.5 \times \ln(\det(R_T) \times s + \det(R_C) \times (1-s)) + 0.5s \times \ln(R_T) + 0.5(1-s) \ln(\det(R_C)). \quad (19)$$

Using formulas (16)–(19), the performance and detection characteristics are calculated. The performance curves shown in Fig. 3–5 are calculated for the case when there is only one target and one clutter, $\sigma_T^2 = \sigma_C^2 = \sigma_N^2 = 1$, and the number of observation periods is $M = 1300$.

In the graphs, the performance curves are also shown for the no-clutter case and for processing that does not use the algorithm presented in the article.

Figure 3 shows curves for different values of target-clutter space and Δd at $\gamma = 1$. The graph shows that processing using the algorithm described in the article improves the detection characteristics even at $\gamma = 1$. With increasing target-clutter space, starting from 10 m, the performance curve approaches to the case when the clutter is completely absent.

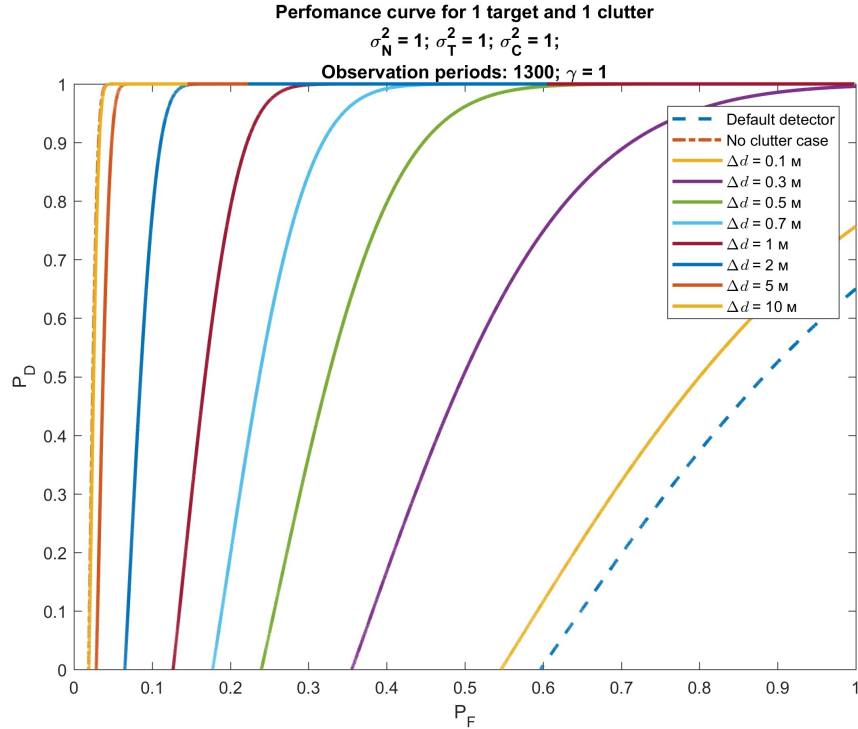


Fig. 3. Performance curves for 1 target and 1 clutter

Fig. 4 shows the curves for different values of γ at $\Delta d = 20$ m. Figure 5 is the zoomed part of Fig. 4. With increasing γ , detection characteristics have a significant gain in comparison with processing without clutter compensation.

Detection characteristics of a multi-element target ($n = 5$) against a background of multiple-element clutter ($N = 5$) for $\sigma_N^2 = 1$, $\sigma_C^2 = \{0.1; 1; 0.1; 0.7; 0.5\}$, $M = 100$, $\gamma = 2$ for different target-clutter location cases (Fig. 6) are shown in Fig. 7.

From the presented curves it follows that with a greater spatial separation of the target and clutters the algorithm significantly increases the detection probability of the target.

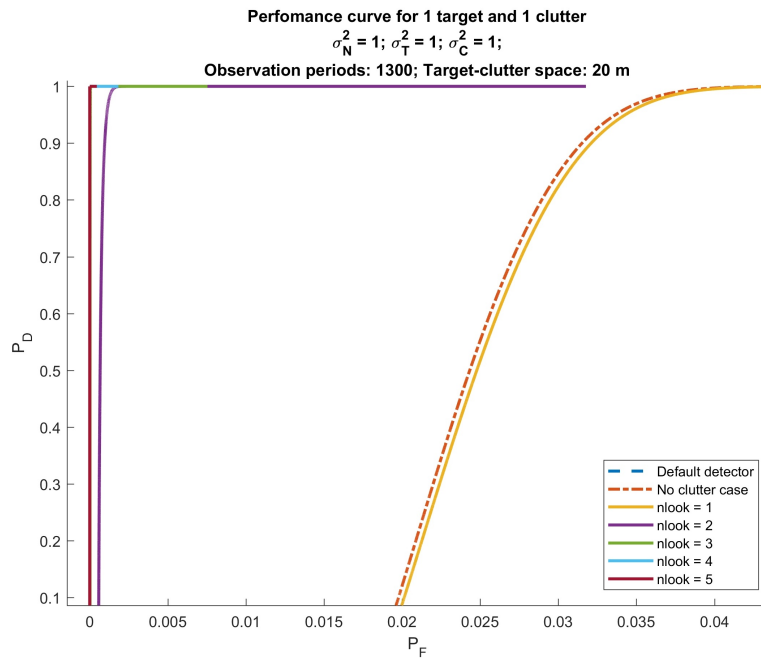


Fig. 4. Performance curves for 1 target and 1 clutter

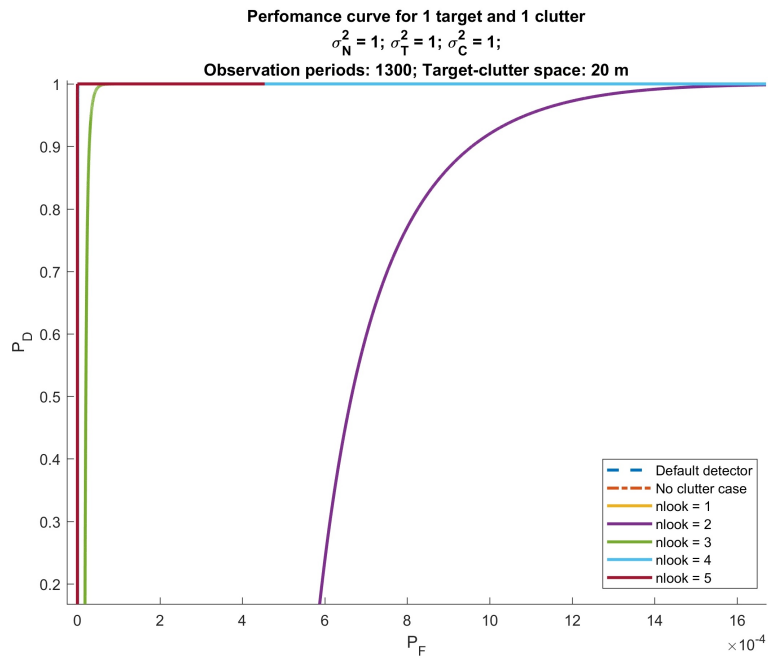


Fig. 5. Performance curves for 1 target and 1 clutter (zoomed)

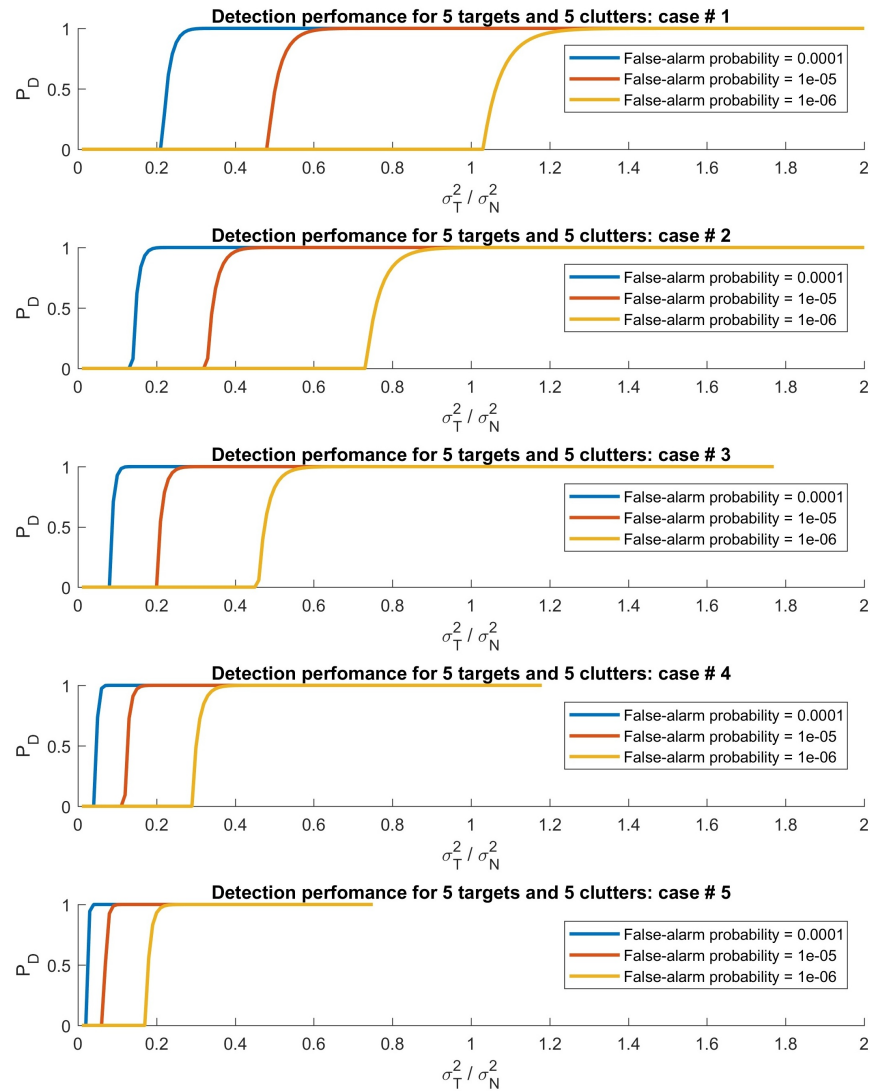


Fig. 6. Detection performance for 5 targets and 5 clutters

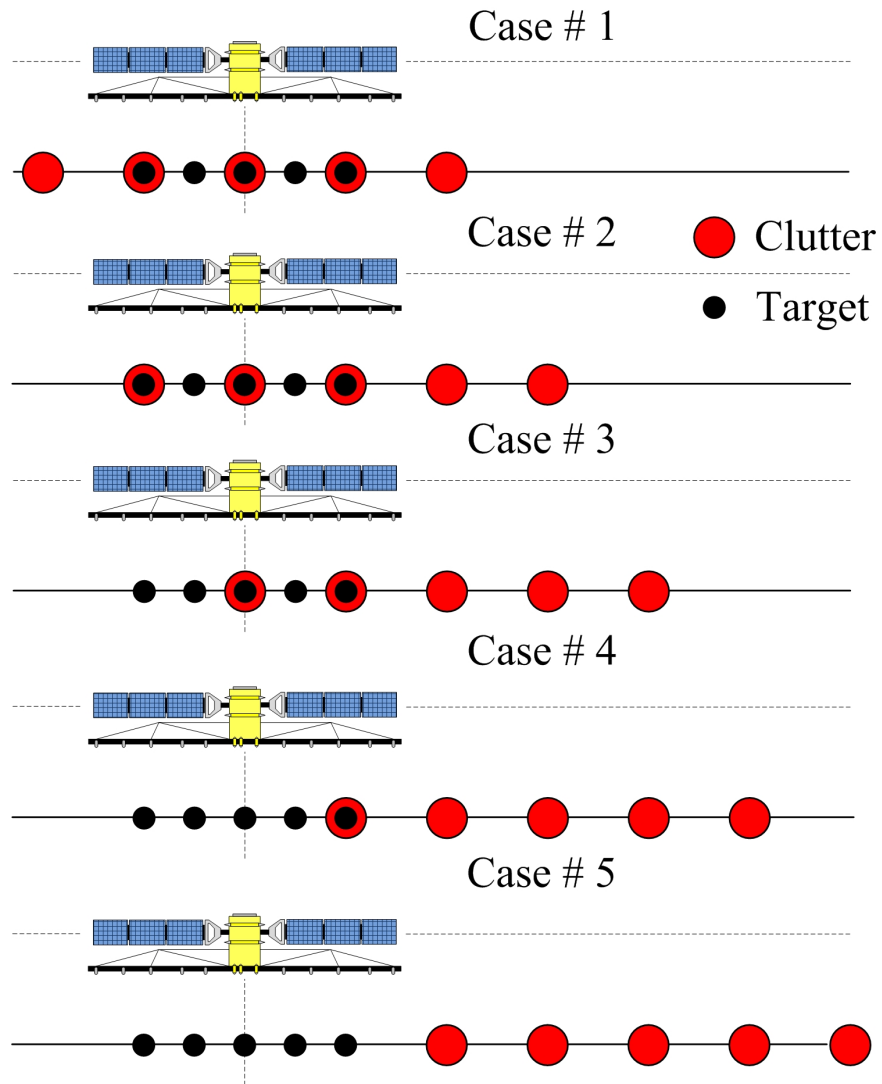


Fig. 7. Target-clutter location cases

4 Conclusion

Clutter reflection suppression algorithm in SAR presented in the article significantly improves the detection efficiency of the signals reflected from targets, which are located closely with clutter objects, even in cases where the clutters overlap targets.

References

1. Dong Yang, Xi Yang, Guisheng Liao: Strong clutter suppression via RPCA in multichannel SAR/GMTI system. *IEEE geoscience and remote sensing letters*. Vol. 12, No. 11 (2015)
2. Baumgartner, S. V.: Fast GMTI algorithm for traffic monitoring based on a priori knowledge. *IEEE transactions on geoscience and remote sensing*. Vol. 50, No. 11 (2012)
3. Dorosinskiy, L. G.: The research of the distributed objects radar image recognition algorithms. *Applied and fundamental studies. Proceedings of the 2st International academic conference*. Vol. 1, 211–214 (2013)